We are IntechOpen, the world's leading publisher of Open Access books Built by scientists, for scientists

6,900
Open access books available

185,000
International authors and editors

200M
Downloads

Our authors are among the

154
Countries delivered to

TOP 1%
most cited scientists

12.2%
Contributors from top 500 universities

Selection of our books indexed in the Book Citation Index in Web of Science™ Core Collection (BKCI)

Interested in publishing with us?
Contact book.department@intechopen.com

Numbers displayed above are based on latest data collected.
For more information visit www.intechopen.com

Dependence of pH Variation on the Structural, Morphological, and Magnetic Properties of Sol-Gel Synthesized Strontium Ferrite Nanoparticles

Muhammad Syazwan Mustaffa,
Rabaah Syahidah Azis and Sakinah Sulaiman

Additional information is available at the end of the chapter

Abstract

In this research work, an attempt of regulating the pH as a sol-gel modification parameter during preparation of $SrFe_{12}O_{19}$ nanoparticles sintered at a low sintering temperature of 900°C has been presented. The relationship of varying pH (pH 1–14) on structural microstructures and magnetic behaviors of $SrFe_{12}O_{19}$ nanoparticles was characterized by X-ray diffraction (XRD), field emission scanning microscope (FESEM), thermogravimetric analysis (TGA), Fourier-transform infrared (FTIR), and vibrating-sample magnetometer (VSM). The single-phase $SrFe_2O_{19}$ with optimum magnetic properties can be obtained at pH 1 with a sintering temperature of 900°C. As pH values increase, the presence of impurity Fe_2O_3 was observed. TGA data-varying pH shows that the total weight loss of most samples was at 30.44% which corresponds to the decomposition process. The IR spectra showed three main absorption bands in the range of 400–600 cm^{-1} corresponding to strontium hexaferrite. SEM micrographs exhibit a circular crystal type of strontium ferrite with an average crystal size in the range of 53–133 nm. A higher saturation magnetization M_s, remanent magnetization M_r, and hysteresis H_c were recorded to have a large loop of 55.094 emu/g, 33.995 emu/g, and 5357.6 Oe, respectively, at pH 11, which make the synthesized materials useful for high-density recording media and permanent magnets.

Keywords: strontium hexaferrite ($SrFe_{12}O_{19}$), sol-gel, pH, structural, magnetic properties

1. Introduction

Ferrite is a magnetic material in the form of ceramic like. Ferrite is usually brittle, hard, iron containing, and generally gray or black in color. It consisted of iron oxides and reacts with

preferable high electrical resistivity of metal oxides. Ferrites have impressive properties such as high magnetic permeability and high electrical resistance [1]. Ferrite magnets have a low hysteresis loss and high intrinsic coercivity [2] which give greater effect in resistance demagnetization from external magnetic field. In addition, a low-cost ferrite magnet has good heat resistance and good corrosion resistance which are useful to many applications like permanent magnet [3, 4], solid-state devices, magnetic recording media [5, 6], microwave device [5], etc. A generic formula of magnetoplumbite structure of ferrite is $MFe_{12}O_{19}$, where M is divalent cations like Ba^{2+} [3, 4], Sr^{2+} [1, 2, 5, 7], and Pb^{2+} [8]. Pullar [9] has mentioned that the best known hexaferrite is those containing divalent cations, because it has preferable high electrical resistivity compared to other types of ferrite. $SrFe_{12}O_{19}$ has been chosen in order to produce a good quality of magnetic recording media due to high electrical resistivity of 10^8 Ω cm [9]. The high coercivity leads to high energy product BH_{max} behavior. Liu [10] has mentioned that a good quality of magnetic recording media should have possible high signal and low noise. In order to meet those criteria, the magnetic materials should have high magnetization; high coercivity but correlated with recording field; single-domain particles or grains; a smaller size of particles or grain size, thermally stable, and therefore a reduced thickness of the active magnetic film of the medium; and a good alignment of the particle or grain easy axis [10]. In recent years, higher levels of recording density have been achieved in the field of magnetic recording. Magnetic tapes employing hexagonal barium ferrite magnetic powder achieve a surface recording density of 29.5 bpsi (bits per square inch). However, when the size of hexagonal ferrite magnetic particles is reduced, the energy for maintaining the direction of magnetization of the magnetic particles (the magnetic energy) tends to become inadequate to counter thermal energy, and thermal fluctuation ends up compromising the retention of recording.

Various techniques are presented for the synthesis of strontium hexaferrite powders such as solid-state synthesis method [11, 12], chemical coprecipitation [13–15], ceramic method [16], and sol-gel [17–19] and hydrothermal methods [20]. The effect of pH variation in this research work via sol-gel method for producing $SrFe_{12}O_{19}$ is key factor for controlling hexaferrite nanostructure and magnetic properties. Other than that, this proposed method has not yet been reported elsewhere in producing $SrFe_{12}O_{19}$ nanoparticles. Recently, the sol-gel route has received considerable attention in the last few years because it has lower calcination temperature, the fact that it also enables smaller crystallites to grow [2]. Sol-gel method produces a better outcome than microemulsion and coprecipitation methods. The sol-gel hydrothermal method combines the advantages of the sol-gel method and the high pressure in the hydrothermal condition [7]. In the hydrothermal process, the particle size and particle morphology can be controlled. $SrFe_{12}O_{19}$ nanoparticles have high purity, ultrafine size, and high coercivity. Some efforts have been carried out to modify the sol-gel process parameters such as pH, basic agent, carboxylic acid, and starting metal salts for further decreasing the calcination temperature and achieving the finer crystallite size [1]. Optimizing the molar ratio of Fe to Sr is very important to produce a single-phase sample, ultrafine particle, and lower calcination temperatures [21]. This ratio varies with the change in starting materials and with the change in method of production [21]. The obtained products that have single-phase particles have a hexagonal shape, the right proportion, and high coercively. The prolonging annealing time

has a significant effect on the high saturation magnetization (M_s), and the high annealing rate formed a highly percentage of pure strontium hexaferrite. Masoudpanah and Ebrahimi [2] state that the preferred molar ratio of Fe/Sr is 10, which is the lowest calcination temperature (800°C) on the formation of single phase of SrM thin films. In addition, XRD showed that the crystallite sizes at a range of 20–50 nm. The magnetic properties of this preferred molar ratio exhibit a good saturation magnetization (267 emu/cm^3), high coercivity (4290 Oe), and a relatively high remanent magnetization (134 emu/cm^3). Minh et al. [7] state that the preferred molar ratio is at 11. The obtained $SrFe_{12}O_{19}$ has high purity, ultrafine size, and high coercivity at H_c = 6315 Oe. This chapter discussed an attempt to employ water as the gel precursor to synthesize nano-sized M-type strontium ferrite ($SrFe_{12}O_{19}$) bulk sample at low sintering temperature 900°C by using a common laboratory chemical. A solution of metal nitrates and citric acid and ammonia has been used to prepare strontium hexaferrite at varying pH.

2. Brief overview of preparation methods

2.1. Raw materials

Strontium nitrate anhydrous granular Sr $(NO_3)_2$ (98%, Alfa Aesar), iron (III) nitrate $Fe(NO_3)_3$ (99%, HmbG), citric acid (CA) $C_6H_8O_7$ (99%, Alfa Aesar), ammonia NH_4OH (25%, SYSTERM), and deionized water were used as starting material in order to synthesize $SrFe_{12}O_{19}$ nanoparticles as listed in **Table 1**.

The general chemical equation for desired $SrFe_{12}O_{19}$ samples is weighed according to the formula:

$$Sr(NO_3)_2 + 12Fe(NO_3)_3 \xrightarrow[NH_4OH]{C_6H_8O_7} SrFe_{12}O_{19} + volatile \qquad (1)$$
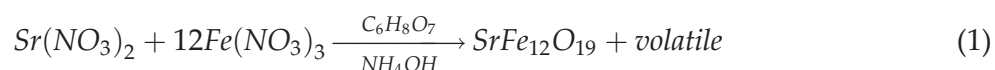
The nitrates were calculated as one mole of $Sr(NO_3)_3$, and 12 moles of $Fe(NO_3)_2$ were needed in order to synthesize one mole of $SrFe_{12}O_{19}$ nanoparticles. In the process of reaction, CA was used as a chelating agent and fuel of combustion. The CA was then calculated according to the molar ratio of citrate to nitrate of 0.75 which first obtained each number of mole nitrate as below:

$$Sr(NO_3)_2 \rightarrow Sr^{2+} + 2(NO_3)^- \qquad (2)$$

$$Fe(NO_3)_3 \rightarrow Fe^{3+} + 3(NO_3)^- \qquad (3)$$
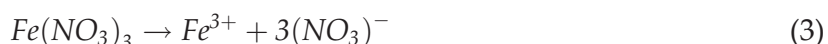
Then, mass of citrate was calculated as:

$$Mass_{CA} = (0.75 \times total\ nitrate) \times molar\ mass_{CA} \qquad (4)$$

In this study, NH_4OH was used to vary the pH value of $SrFe_{12}O_{19}$ in order to study the effect of pH value in its morphology and magnetic properties.

Chemical name	Compound formula	Molecular weight (g/mol)	Weight ratio (g)
Strontium nitrate anhydrous (salt)	$Sr(NO_3)_2$	211.63	0.4183
Iron (III) nitrate	$Fe(NO_3)_3$	403.84	9.5817
Citric acid (powder)	$C_6H_8O_7$	191.12	11.8368
Ammonia	NH_4OH	35.04	Varied depend on pH Measured by pH meter

Table 1. Compound used for sol-gel synthesis.

2.2. Sample preparation and characterizations

An appropriate amount of $Sr(NO_3)_2$, $Fe(NO_3)_3$, and $C_6H_8O_7$ was dissolved in 100 ml of deionized water for 30 min at 50°C with constant stirrer rotation of 250 rpm. The mixtures were continuously stirred, and NH_4OH was added in order to vary the pH from pH 1–14 which is measured by HI 2211 pH/ORP meter (HANNA instruments). The solutions then were stirred on the hot plate for 24 h at 60°C. The solution was left in oven at temperature of 80°C for 2 days to turn the solution into a sticky gel. The sticky gel was stirred again stirred on hot plate, and the temperature was increased up to 150°C to dehydrate and form a powder. The powder formed were crushed by using mortar before sintering it at 900°C for 6 h with the heating rate of 3.5°C/min. The crystalline structural characterization of XRD was performed using a Philips X'Pert X-ray diffractometer model 7602 EA Almelo with Cu Kα radiation at 1.5418 Å. The range of diffraction angle used is from 20 to 80° at room temperature. The accelerating current and working voltage were 35 mA and 4.0 kV, respectively. The data are then analyzed by using X'Pert Highscore Plus software. The lattice constant, *a*, is obtained by Eq. (5):

$$a = d\sqrt{h^2 + k^2 + l^2} \tag{5}$$

Where *d* is the interatomic spacing and (*h k l*) are miller indices. The volume cell V_{cell} was calculated using Eq. (6):

$$V_{cell} = \frac{\sqrt{3}}{2}a^2c \tag{6}$$

Where *a* and *c* are lattice constants. The theoretical density ρ_{theory} of sample was calculated using Eq. (7):

$$\rho_{theory} = \frac{2M}{N_A V} \tag{7}$$

Where *M* is molecular weight of $SrFe_{12}O_{19}$, which is equal to 1061.765 g. The weight of two molecules in one unit cell is $2 \times 1061.765 = 2123.53$ g; N_A is the Avogadro's number (6.022×10^{23} mol^{-1}). The porosity *P* of the samples can be calculated using Eq. (8):

$$P = \left(\frac{1 - \rho_{\text{exp}}}{\rho_{\text{theory}}} \right) \times 100\% \qquad (8)$$

Where ρ_{exp} is the experimental density and ρ_{theory} is the xrd density.

Meanwhile, the crystallite size can be measured by using the Scherrer equation (Eq. 9):

$$D = \frac{k\lambda}{\beta \cos \theta} \qquad (9)$$

Where D is crystallite size, k is the Scherrer constant value of 0.94, λ is Cu Kα radiation wavelength of 1.542 Å, β is half-peak width of diffraction band, and θ is the Bragg angle corresponding to the planes.

The thermal stability of these samples was obtained by using TGA/SDTA 851 of Mettler Toledo thermogravimetric analyzer. The sample weighted about 10 mg was used at operating temperature range from 0 to 1000°C with heating rate 5°C/min. Fourier-transform infrared by Perkin Elmer model 1650 was used to determine the infrared spectrum of absorption and emission bands of sample. It was performed between infrared spectra of 280–4000 cm^{-1} with resolution of 4 cm^{-1}. The micrograph of microstructure was observed using a FEI Nova NanoSEM 230 machine to study the morphology and microstructure of solid material. The sample was prepared in bulk pallet at a diameter of 1 cm and coated with gold in order to avoid charge buildup as the electron beams are scanned over the samples' surface. The distribution of grain size image was fixed at magnification of 100,000X with 5.0 kV. The distribution of average grain size of microstructure was calculated by using these images. The distributions of grain sizes were obtained by taking at least 200 different grain images for the sample and estimating the mean diameters of individual grains by using the J-image software. The magnetic properties of samples were measured by VSM Model 7404 LakeShore. The measurement was carried out in the room temperature with sample weight about 0.2 g. The external field applied was 12 kOe parallel to the sample. From this analysis, saturation magnetization, M_s; remanent magnetization, M_r; and coercivity, H_c, were recorded, and the hysteresis loop was plotted.

3. Research findings and outcomes

3.1. Structural analysis

Figure 1 shows the XRD spectra of the samples sintered at 900°C with different pH values (pH 1–14). The XRD spectrum shows the formation of a single phase of SrFe$_{12}$O$_{19}$ nanoparticles. The structure of XRD peaks was referred to standard strontium hexaferrite (SrFe$_{12}$O$_{19}$) with JCPDS reference code of 98002-9041 [22], with hexagonal crystal system belonging to space group of *P63/mmc* that proved the hexagonal crystal structure system formation. The SrFe$_{12}$O$_{19}$ phase formed with miller indices shown as [110], [008], [017], [114], [021], [018], [023], [116],

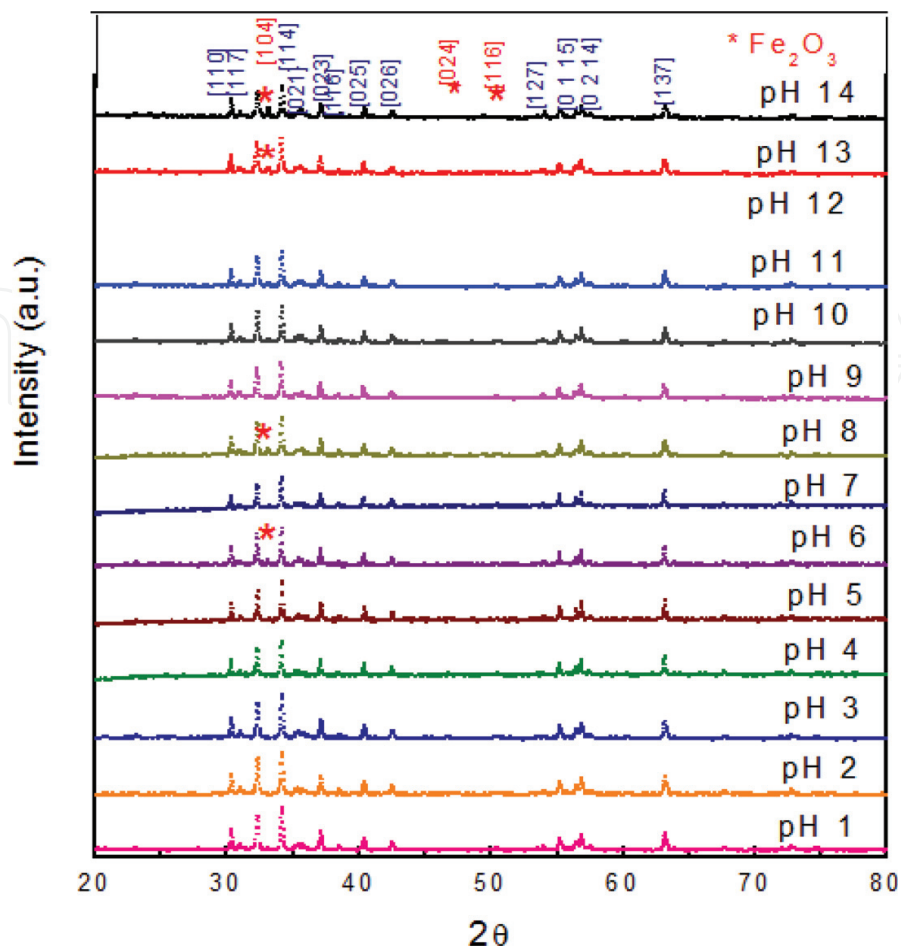**Figure 1.** The X-ray diffraction spectra of SrFe$_{12}$O$_{19}$ nanoparticles for pH 1–14 sintered at 900°C.

[025], [026], [127], [034], [0211], [0115], [0214], and [137], respectively. The highest intensity can be observed at 2θ (34.218°) with miller indices of [114] of reference index code of 98-002-9041 [22]. However, as pH increases, the amount of ammonia required increases. This factor leads to the formation of hematite (Fe$_2$O$_3$) in pH 6, pH 8, pH 13, and pH 14 due to excess ammonia that could not completely vanish during reaction. The formation of Fe$_2$O$_3$ occurred at 2θ = 33.139 and 49.673° with miller indices of [104] and [024]. The hematite Fe$_2$O$_3$ patterns were indexed to ICSD reference code of 98-005-3678 [23]. It was explained by Masoudpanah and Ebrahimi [2] that the increasing pH of the sol results in the absorption of positively charged Sr ions on iron gels and the formation of negatively charged iron gels. A single-phase SrFe$_{12}$O$_{19}$ was obtained at a low sintering temperature of 900°C for powder pH which proves the benefit of using sol-gel method in this SrFe$_{12}$O$_{19}$ reaction. It was agreed that obtained single phase of SrFe$_{12}$O$_{19}$ at lower temperature was due to the solubility of Sr (NO$_3$)$_2$ that decreases at elevated temperatures [24]. Hence, more Sr^{2+} ions are needed for the formation of the strontium hexaferrite [2]. The diffusion rates increased in the nonstoichiometric mixtures because of the induced lattice defects which could be observed from lower lattice parameter [2].

The average crystallite size (**Table 2**) determined from the full width at the half maximum (FWHM) of the XRD patterns was calculated using the Scherrer formula provided from X'Pert

pH	Peak pos. 2θ (°)	Miller indices (hkl)	Peak width (°)	Space group	Lattice constant		V_{cell} (nm^3)	ρ_{xrd} (g cm^{-3})	ρ_{exp} (g cm^{-3})	P (%)	Calculated crystalline size, D (nm)
					a (Å)	c (Å)					
1	34.20	[114]	0.13	$P63/mmc$	5.883	23.018	5.11	4.634	13.899	0.690	63.226
2	34.21	[114]	0.13	$P63/mmc$	5.882	23.051	5.11	4.399	11.217	0.691	63.228
3	34.22	[114]	0.16	$P63/mmc$	5.882	23.051	5.11	3.832	8.077	0.691	51.372
4	34.20	[114]	0.16	$P63/mmc$	5.884	23.058	5.10	4.693	13.237	0.691	51.369
5	34.25	[114]	0.16	$P63/mmc$	5.880	23.040	5.11	4.200	12.114	0.690	51.376
6	34.18	[114]	0.16	$P63/mmc$	5.884	23.060	5.10	4.492	11.831	0.691	51.366
7	34.18	[114]	0.18	$P63/mmc$	5.884	23.057	5.10	4.497	12.368	0.691	45.661
8	34.17	[114]	0.18	$P63/mmc$	5.885	23.058	5.10	3.419	9.633	0.691	45.660
9	34.12	[114]	0.14	$P63/mmc$	5.889	23.025	5.10	4.633	9.153	0.691	57.266
10	34.19	[114]	0.15	$P63/mmc$	5.884	23.047	5.10	4.784	6.254	0.691	54.685
11	34.18	[114]	0.15	$P63/mmc$	5.885	23.053	5.10	4.721	7.435	0.691	53.231
12	34.22	[114]	0.17	$P63/mmc$	5.880	23.030	5.12	4.699	8.125	0.689	47.762
13	34.14	[114]	0.18	$P63/mmc$	5.884	23.066	5.10	4.705	7.736	0.691	46.693
14	34.20	[114]	0.18	$P63/mmc$	5.882	23.023	5.11	4.612	9.782	0.690	46.941

Table 2. The summary of the of SrFe$_{12}$O$_{19}$ nanoparticles for pH 1–14.

Highscore Plus software. From the plotted crystallite size relationship with pH of samples (**Figure 2**), it shows two groups of crystallite size distribution: acidic group (1) for pH 1–8 and alkaline group (2) for pH 9–14. Both groups show an improvement of crystallinity that gives out smaller crystallite size as the pH increases, which results in smaller grain size as the crystallite size increases.

The lattice constant *a* and *c* values (**Table 2**) observed were not far different from the theoretical SrFe$_{12}$O$_{19}$ lattice constant, where *a* = 5.8820 Å and *c* = 23.0230 Å [25], as similar as reported by
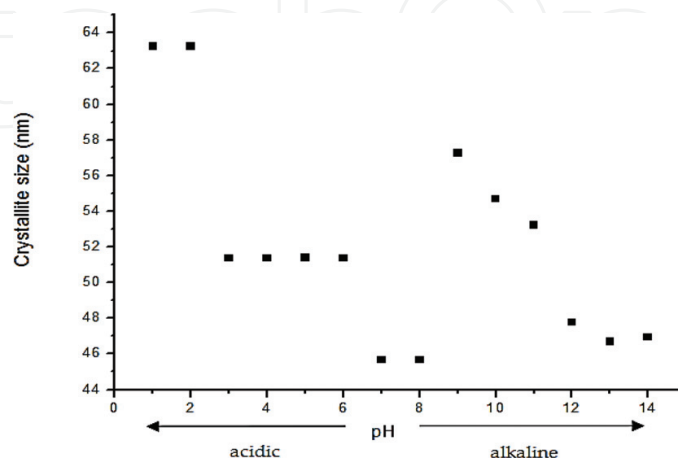

Figure 2. Relationship of crystallite size versus pH.

Masoudpanah et al. [2, 26] and Dang et al. [27]. There is a slight increment in lattice constant c as pH increases and fluctuated data of lattice constant a. It is shown that, at pH 10, the lattice constant a of 5.884 Å was the highest peak with a lower peak of lattice constant c of 23.047 Å. The standard strontium hexaferrite ($SrFe_{12}O_{19}$) with JCPDS reference code of 98-002-9041 [22] has theoretical density of 5.11 g cm^{-3} [25]. Theoretically, the density of the sample, ρ_{EXP}, is affected by the lattice constants a and c. The lattice parameter a and c values observed were not far different from the theoretical $SrFe_{12}O_{19}$ lattice constant, where a = 5.8820 Å and c = 23.0230 Å (**Figure 3**) [25]. The a and c parameters observed are similar to Masoudpanah et al. [2] and Dang et al. [27].

The lattice constant was fluctuated around the theoretical lattice constant. However, in the experiment, the density was more affected by the preparation of the sample which results in porosity of the sample. The distant the difference of density of XRD (ρ_{XRD}) and experimental density (ρ_{EXP}), the higher the number of porosity, which results in reducing the mass of the pallet sample by pores. The highest density value for ρ_{XRD} is at pH 12 (5.1148 gcm^{-3}), and the highest density value for ρ_{EXP} is at pH 10 (4.784 gcm^{-3}). The porosity occurs because of the presence of pores in the samples as a result after sintering of bulk samples. The pores occur due to an error from preparing sample and the loosen powder while pressing the sample using hydraulic presser. As the ρ_{EXP} approaches to the ρ_{XRD}, the pores' percentage becomes lower. The highest porosity of 13.24% was found at pH 4 with ρ_{XRD} of 5.1001 g cm^{-3} and ρ_{EXP} of 4.425 g cm^{-3}. Meanwhile, pH 10 exhibits a lower porosity of 6.254% with ρ_{XRD} of 5.1032 g cm^{-3} and ρ_{EXP} of 4.784 g cm^{-3} (**Table 2**).

The powder was synthesized using a control molar ratio of 1:12 with respect to strontium and nitrate. However, the sample with various pH was prepared with an addition of nitrate into the solution. The sample ratio of Sr (NO_3)$_3$ and Fe(NO_3)$_2$ is (Fe/Sr) = 12:1, and the samples were sintered at 900°C. From previous work reported, a single phase of strontium ferrite ($SrFe_{12}O_{19}$) was obtained for samples sintered at 850°C with Fe/Sr molar ratio of 11.5 via sol-gel route [28].
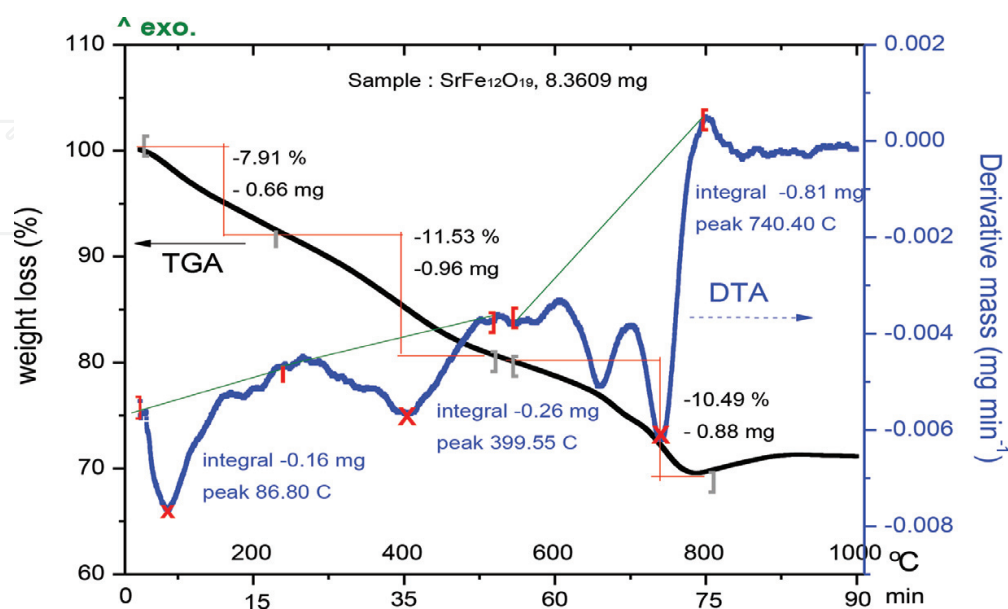

Figure 3. The TGA and DTA traces for dried powder of $SrFe_{12}O_{19}$ sintered up to 1000°C.

Masoudpanah and Ebrahimi [2] found a single phase of $SrFe_{12}O_{19}$ at sintering temperature of 900°C prepared using sol-gel technique. In general, the lowest sintering temperature of $SrFe_{12}O_{19}$ is around 800–1000°C. Hence, the raw powder (non-sintered) was tested by TGA to identify the best temperature by sintering up to 1000°C. The TGA curves as plotted in **Figure 3** show a decreasing amount of weight as the powder sintered up to 1000°C in 20 min with a starting weight of 8.3609 mg. Meanwhile, the DTA diagrams reveal three peaks shown at range 86.80–100, 399.55, and 740.40°C due to decomposition process. At a constant heating rate, the endothermic peak at 86.80–100°C had −7.91% of weight loss due to the dehydration of the absorbed water as the powder slowly turns into burnt gel [2]. The first exothermic peak at 399.55°C with a weight loss of −11.53% is due to the elimination of the organic compound which tends to the decomposition of NH_4NO_3 that liberates NO, O_2, and H_2O [2]. Meanwhile, at stage 740.40°C, the exothermic peak with a weight loss of −10.49% shows the decomposition of citric acid and the breakdown of the Fe_2O_3 to Fe as reported [17]. The stable temperature is at 880°C which permits the completeness of reaction. Hence, sintering temperature at 900°C was used in this work.

Figure 4 shows the FTIR spectra of $SrFe_{12}O_{19}$ nanoparticles for pH variation (pH 1–14), with IR range of 400–4000 cm^{-1}. It is noticeable that spectrum appeared in the range of 430, 583, 904, and 1446 cm^{-1} of IR characteristic band. The stretching band of CH_2 appeared at 436 cm^{-1} attributed to the presence of CH saturated compound, which has been agreed by [29]. The vibration of CH bond could be due to the chemical reaction in a process of hexagonal structure form, where the CH bond of citric acid loses their CH bond. The spectrum of metal-oxygen vibration of Sr–O Fe–O was found at 583 cm^{-1} [26]. Masoudpanah and Ebrahimi [2] explained that an occurred reaction between citric acid and ferric ions is attributed to the stretching mode
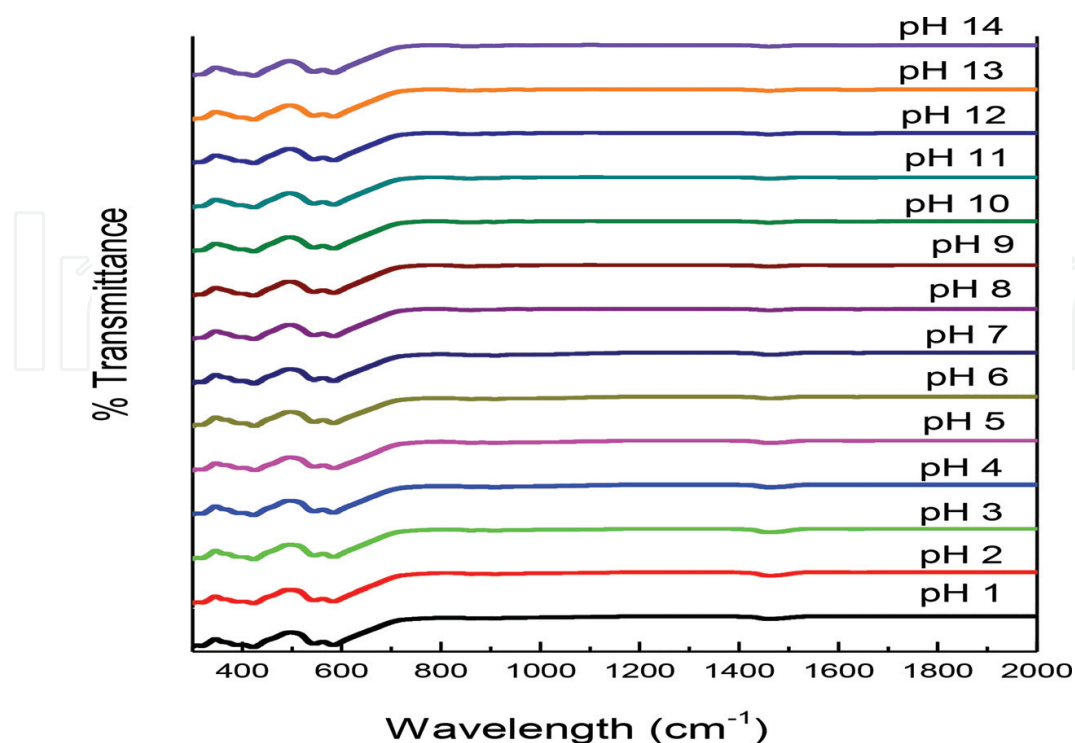

**Figure 4.** FTIR spectra of $SrFe_{12}O_{19}$ for pH variation sintered at 900°C.

of Fe–O, which confirms the formation of chelate in sol-gel route. It is proven by many researchers who claim that the absorption bands at range 443–600 cm^{-1} were results of the formation of strontium ferrite as the stretching vibration of metal-oxygen bond of Sr–O Fe–O occurs [30–33]. All pH reveals these two bond bands. However, there were some reducing and vanished bands in the next bond bands at 904 and 1460 cm^{-1}. It is due to the purity of $SrFe_{12}O_{19}$ nanoparticles, as there was some interruption of Fe_2O_3 in the sample as shown in **Figure 1** and **Table 2**. In this study, pH 8, pH 10, pH 13, and pH 14 come out with a percentage of hematite, Fe_2O_3. First, the pure $SrFe_{12}O_{19}$ (pH 1–7, pH 9, pH 11–12) had a relatively strong and broad bands at peak 904 cm^{-1}, which revealed that there was amine functional group for N–H vibration due to decomposition of NH_3. Pereira et al. [32] stated that this broad vibration of Sr–O stretching indicates the formation of strontium nanoferrites. It is agreed by Sivakumar et al. [34] that the strontium ferrite was formed and the iron oxide vanished at 900 cm^{-1}. Meanwhile, pH 6, pH 8, pH 13, and pH 14 show a relative small vibration band at 904 cm^{-1} due to the presence of Fe_2O_3. As pH increases up to pH 14, the amount of ammonia increases gradually. Excess amount of ammonia failed to completely decompose the NH_3 bonds and break down the N–H vibration. Lastly, the absorption bands at 1446 cm^{-1} found in pure pH sample were attributed to the vibrating bands of Fe-O-Fe due to the decomposition of metal with oxide band [29]. There was some significant data that show in pH 9, pH 11, and pH 12, as a single phase of samples is formed as pH increased.

3.2. Microstructural analysis

The microstructure and grain size distribution of bulk $SrFe_{12}O_{19}$ nanoparticles are shown in **Figure 5**. The grain size seems to have agglomerated and charged nanoparticles when increasing the pH value. The grain size was found in the range of 53.22–133.25 nm. The pH 4 produces pores of 13.24%. Meanwhile, the most packed grains are for sample at pH 10, with porosity of 6.25% (**Table 2**). The microstructure shows that some of the samples have a large porosity due to the presence of polyvinyl alcohol during the preparation of pellet bulk $SrFe_{12}O_{19}$ nanoferrites. The histogram of the grain distribution was shifted from small grain sizes to exhibiting larger grains from pH 1 to 8. Nevertheless, the grain size was observed to be decreasing as the pH is reaching 9–14 (**Table 3**).

3.3. Magnetic behaviors

The development of *M-H* hysteresis loop at various pH is illustrated in **Figure 6**. The magnetic saturation, M_s; remanent magnetization, M_r; coercivity, H_c; grain size; and porosity of $SrFe_{12}O_{19}$ nanopowder are shown in **Table 4**. An obvious erect, larger, and well-defined hysteresis loop can be observed. It is probably due to the strong ferromagnetic behavior, indicating the formation of $SrFe_{12}O_{19}$ nanoparticles with high volume fraction of the complete crystalline $SrFe_{12}O_{19}$ phase. Thus a strong interaction of magnetic moments within domains occurred due to exchange forces. This observed phenomenon can be considered as ordered magnetism in the sample. In fact, in order to obtain an ordered magnetism and well-formed
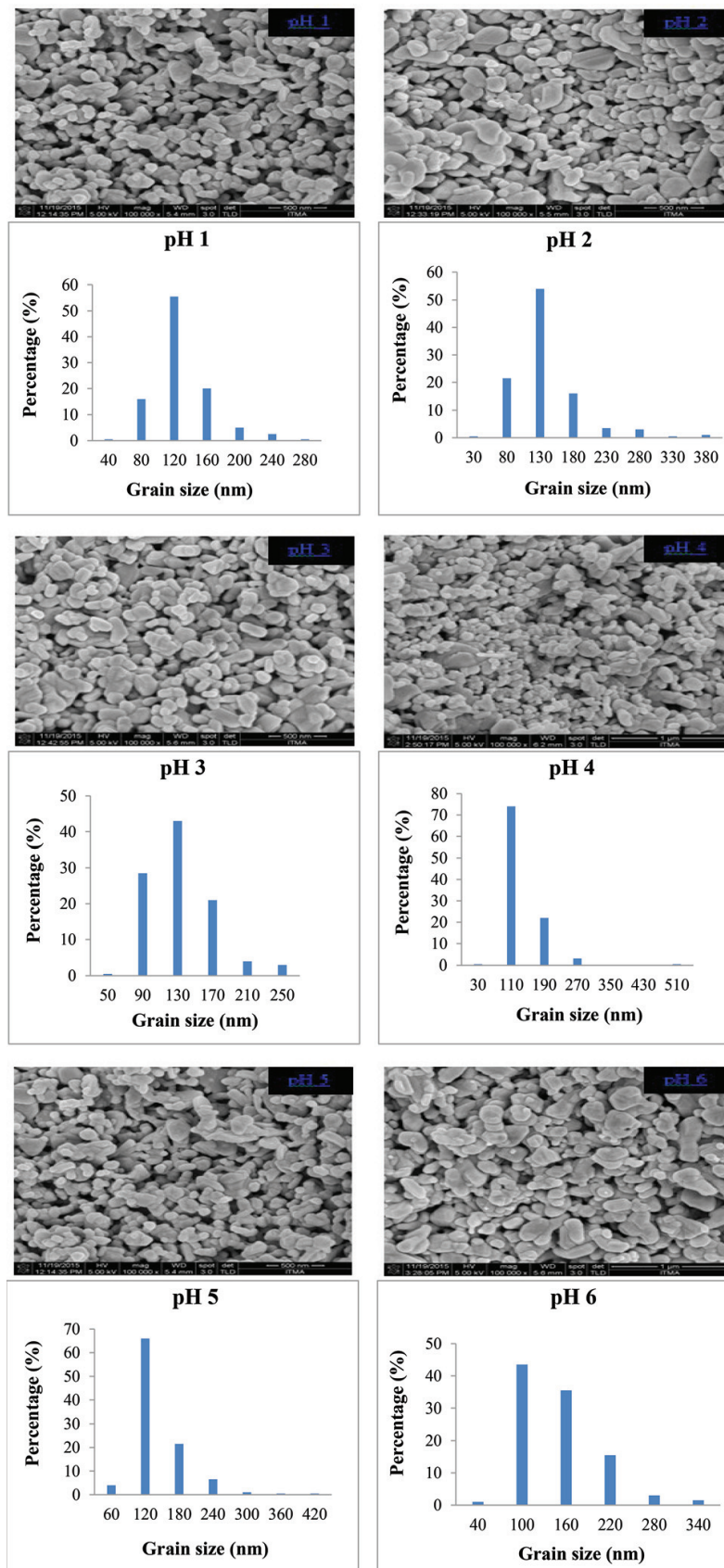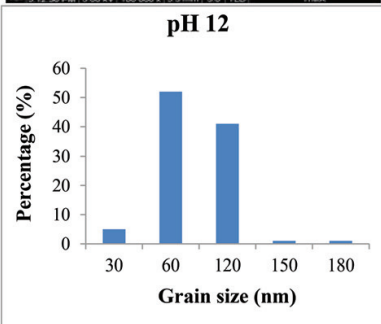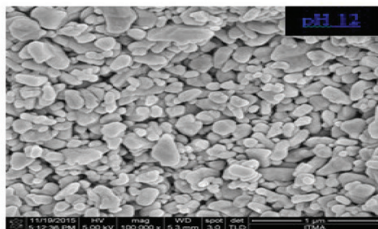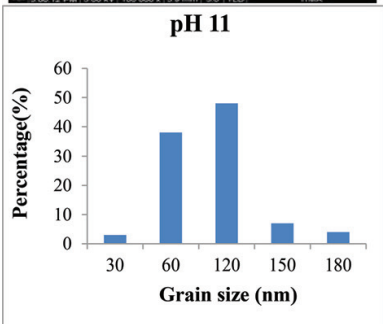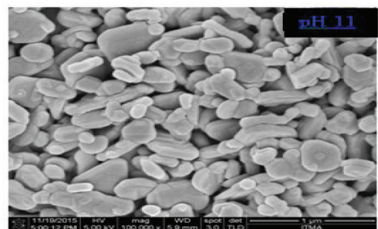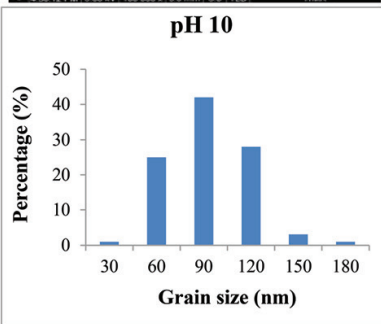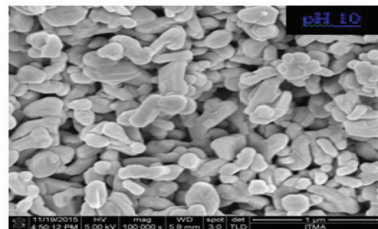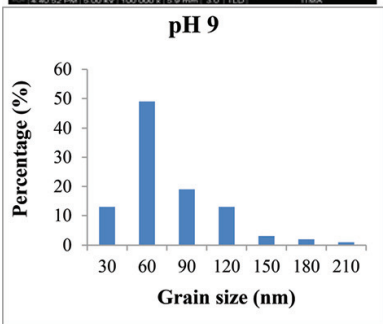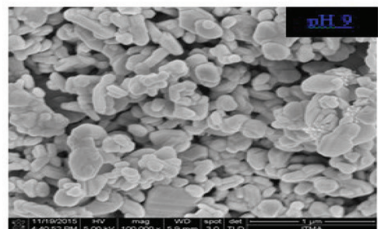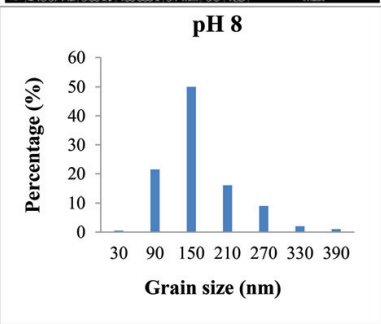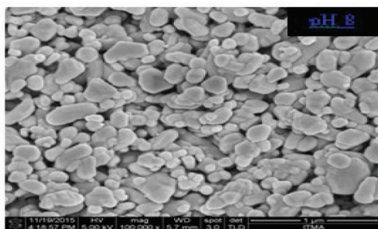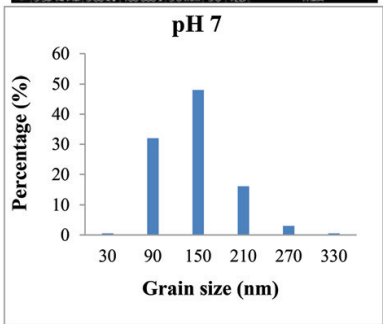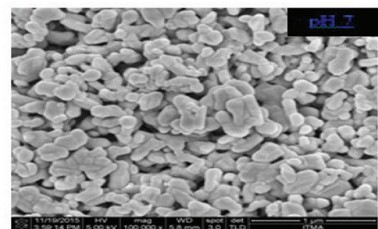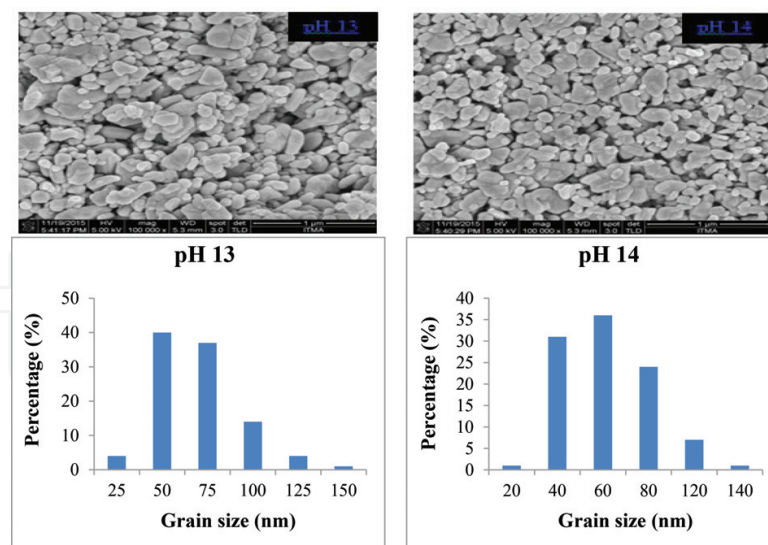
Figure 5. The micrograph image and grain size distribution of $SrFe_{12}O_{19}$ sintered at 900°C by varying pH value.

pH	Grain size (nm)
1	108
2	114
3	115
4	96
5	111
6	120
7	116
8	133
9	61
10	79
11	75
12	62
13	57
14	53

Table 3. Grain size of $SrFe_{12}O_{19}$ sintered at 900°C by varying pH value.

M-H hysteresis loop, there must exist a significant domain formation, a sufficiently strong anisotropy field (H_a), and optional addition contributions, which come from defects such as grain boundaries and pores [35]. The saturation magnetization (M_s), remnant magnetization (M_r), and coercivity (H_c) are found to decrease with increasing pH by addition of ammonia in the sol-gel precursor. From the previous study, the H_c is 4290 Oe, obtained at pH 7 [2, 26]. The
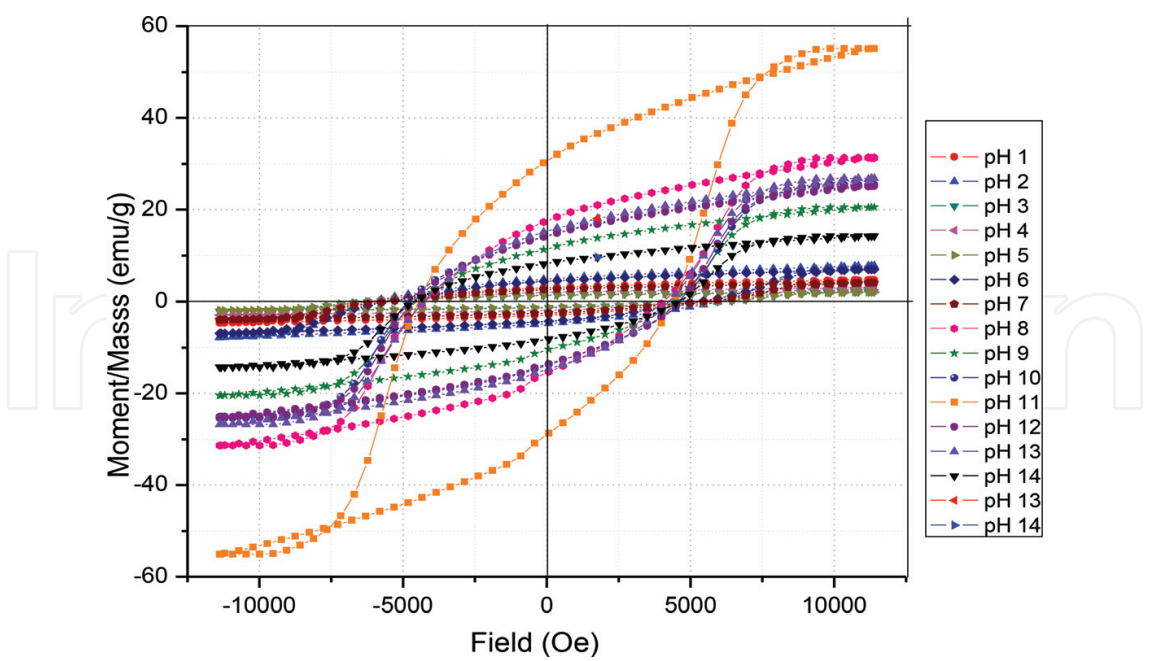
Figure 6. The *M-H* hysteresis loop $SrFe_{12}O_{19}$ of pH 1–14 sintered at 900°C.

pH	Saturation magnetization, M_s (emu/g)	Remnant magnetization, M_r (emu/g)	Coercivity, H_c (Gs)
1	4.776	3.001	6094.7
2	7.822	4.870	6005.8
3	2.168	1.373	5966.1
4	3.006	1.929	5808.6
5	2.016	1.309	6074.8
6	7.022	4.416	5377.0
7	4.028	2.554	5461.2
8	31.342	19.363	5058.3
9	20.488	12.776	5422.2
10	25.471	15.825	5663.1
11	55.094	33.995	5357.6
12	25.114	15.674	5532.7
13	26.849	16.885	5185.9
14	14.239	9.1325	5520.7

Table 4. M_s, M_r and H_c of $SrFe_{12}O_{19}$ as a function of pH.

microstructures of nanoparticles were affected by the increase of pH value. This is in agreement with findings reported by Yang et al. [36], where the formation of particles became larger [37] with the increase of pH from 5 to 11. This is due to the aggregation of small particle that

occurs when there is a strong magnetic interaction between magnetic atoms (Fe or Co) containing in Co-Fe-Al grains as the composition of Co increases and the composition of Al decreases [38]. In this work, it is noticeable that pH 11 has the largest hysteresis loops as well as high magnetic properties. Moreover, the remaining pH exhibit almost the same hysteresis loop with a slight change in M_s and M_r. Meanwhile, the presence of Fe_2O_3 impurity in the samples of pH 6, 8, 13, and 14 shows a decrease in H_c, which affects the crystalline and grain boundary. The H_c is observed to reduce as pH increased. The presence of intragranular trapped pores in the grains was due to rapid grain growth of sample. The presence of intragranular pores would pin down the magnetic moment in grains, thus reducing the M_s and also the H_c. The decrease in H_c as pH increases can be attributed to the decrement of magnetocrystalline anisotropy with anisotropic Fe^{2+} ions located in a 2A site, and the enlargement of the grain size is evident in FESEM micrographs (**Figure 5**). The M_s and M_r are also observed to decrease as pH increases. The decrement of magnetic parameters as pH increases could be due to the existence of large amount of diamagnetic phases as the amount of ammonia NH_3 increases. It seems that the main roles of the diamagnetic NH_3 are to isolate Sr-ferrite nanoparticles from each other, thus reducing exchange interaction between them, and are known to have a detrimental effect on M_s and M_r.

4. Conclusions

Single-phase $SrFe_2O_{19}$ ferrite nanoparticles were successfully synthesized by sol-gel citrate-nitrate method. From the discussion presented earlier, the influence of pH variation on the $SrFe_2O_{19}$ ferrite nanoparticles on the structural, microstructural, and magnetic properties was discussed. An increment amount of ammonia has changed the purity, average grain size, density, and its porosity, which affected the magnetic properties of the samples. Those charac-teristics reveal an understanding on how important effects of pH study (linear effect of pH and acidic-alkaline effect) underlining on $SrFe_{12}O_{19}$ nanoparticles, as most researchers neglect it.

Acknowledgements

Conflict of interest

The authors declare that they have no competing interest.

Author details

Muhammad Syazwan Mustaffa[2], Rabaah Syahidah Azis[1,2]* and Sakinah Sulaiman[1]

*Address all correspondence to: rabaah@upm.edu.my

1 Materials Synthesis and Characterization Laboratory, Institute of Advanced Technology, Universiti Putra Malaysia, Serdang, Selangor, Malaysia

2 Department of Physics, Faculty of Science, Universiti Putra Malaysia, Serdang, Selangor, Malaysia

References

[1] Masoudpanah SM, Ebrahimi SAS, Ong CK. Preparation of strontium hexaferrite film by pulsed laser deposition with *in situ* heating and post annealing. Journal of Magnetism and Magnetic Materials. 2012;**324**(18):2894-2898. DOI: 10.1016/j.jmmm.2012.04.034

[2] Masoudpanah SM, Ebrahimi SAS. Synthesis and characterization of nanostructured strontium hexaferrite thin films by the sol-gel method. Journal of Magnetism and Magnetic Materials. 2012;**324**(14):2239-2244. DOI: 10.1016/j.jmmm.2012.02.109

[3] Perdamean S, Muljadi M, Siregar RT, Tomi BW. Ferrite-based material as a permanent magnet for components of electrical generators. Advances in Natural Sciences: Nanoscience and Nanotechnology. 2011;**2**:045016. DOI: 10.1088/2043-6262/2/4/045016

[4] Topal U, Bakan HI. Permanently magnetic $BaFe_{12}O_{19}$ foams: Synthesis and characterization. Materials Chemistry and Physics. 2010;**123**(1):121-124. DOI: 10.1016/j.matchemphys.2010.03.070

[5] Ashiq MN, Iqbal MJ, Najam-Ul-Haq M, Hernandez Gomez P, Qureshi AM. Synthesis, magnetic and dielectric properties of ErNi doped Sr-hexaferrite nanomaterials for applications in high density recording media and microwave devices. Journal of Magnetism and Magnetic Materials. 2012;**324**(1):15-19. DOI: 10.1016/j.jmmm.2011.07.016

[6] Hibst H, Schwab E. Magnetic recording materials. Materials Science and Technology. Federal Republic of Germany: WILEY-VCH Verlag GmbH & CoKGaA; 2006. DOI: 10.1002/9783527603978.mst0041

[7] Minh T, Dang H, Trinh VD, Bui DH. Sol-gel hydrothermal synthesis of strontium hexaferrite nanoparticles and the relation between their crystal structure and high coercivity properties. Advances in Natural Science and Nanotechnology. 2012;**3**(2):1-7. DOI: 10.1088/2043-6262/3/2/025015

[8] Singhal S, Namgyal T, Singh J, Chandra K, Bansal S. A comparative study on the magnetic properties of $MFe_{12}O_{19}$ and $MAlFe_{11}O_{19}$ (M = Sr, Ba and Pb) hexaferrites with different

morphologies. Ceramics International. 2011;**37**(6):1833-1837. DOI: 10.1016/j.ceramint.2011. 02.001

[9] Pullar RC. Hexagonal ferrites: A review of the synthesis, properties and applications of hexaferrite ceramics. Progress in Materials Science. 2012;**57**(7):1191-1334. DOI: 10.1016/j. pmatsci.2012.04.001

[10] Liu JP, Fullerton E, Gutfleisch O, Sellmyer DJ. Nanoscale Magnetic Materials and Applications. London, New York: Springer Dordrecht Heidelberg; 2010. DOI: 10.1007/978-0-387-85600-1

[11] Sharma P, Rocha RA, Medeiros SN, Hallouche B, Paesano A. Structural and magnetic studies on mechanosynthesized $BaFe_{12-x}Mn_xO_{19}$. Journal of Magnetism and Magnetic Materials. 2007;**316**:29-33. DOI: 10.1016/j.jmmm.2007.03.207

[12] Sánchez-DeJesús F, Bolarín-Miró AM, Cortés-Escobedo CA, Valenzuela R, Ammar S. Mechanosynthesis, crystal structure and magnetic characterization of M-type $SrFe_{12}O_{19}$. Ceramics International. 2014;**40**:4033-4038

[13] Luo J. Structural and magnetic properties of Nd-doped strontium ferrite nanoparticles. Materials Letters. 2012;**8**:162-164

[14] Faloh-Gandarilla JC, Dıaz-Castanon S, Watts BE. Magnetization reversal and interactions in $SrFe_{12}O_{19}$. Physica Status Solidi B. 2016;**254**(4):1-7. https://doi.org/10.1002/pssb.201600393

[15] Ashiq MN, Iqbal MJ, Gul IH. Structural, magnetic and dielectric properties of Zr-Cd substituted strontium hexaferrite ($SrFe_{12}O_{19}$) nanoparticles. Journal of Alloys and Compounds. 2009;**487**:341-345

[16] Kostishyn VG, Panina LV, Kozhitov LV, Timofeev AV, Kovalev AN. Synthesis and multiferroic properties of M-type $SrFe_{12}O_{19}$ hexaferrite ceramics. Journal of Alloys and Compounds. 2015;**645**:297-300

[17] Wong YC, Wang J, Teh GB. Structural and magnetic studies of $SrFe_{12}O_{19}$ by sol-gel method. Procedia Engineering. 2014;**76**:45-52. DOI: 10.1016/j.proeng.2013.09.246

[18] Zhang Z, Liu X, Wang X, Wu Y, Li R. Effect of Nd-Co substitution on magnetic and microwave absorption properties of $SrFe_{12}O_{19}$ hexaferrites. Journal of Alloys and Compounds. 2012;**525**:114-119

[19] Afghahi SSS, Peymanfar R, Javanshir S, Atassi Y, Jafarian M. Synthesis, characterization and microwave characteristics of ternary nanocomposite of MWCNTs/doped Sr-hexaferrite/PANI. Journal of Magnetism and Magnetic Materials. 2016;**423**:152-157

[20] Xia A, Zuo C, Chen L, Jin C, Lv Y. Hexagonal $SrFe_{12}O_{19}$ ferrites: Hydrothermal synthesis and their sintering properties. Journal of Magnetism and Magnetic Materials. 2013;**332**(4): 186-191

[21] Mirkazemi SM, Alamolhoda S, Ghiami Z. Erratum to: Microstructure and magnetic properties of $SrFe_{12}O_{19}$ nano-sized powders prepared by sol-gel auto-combustion method with

CTAB surfactant. Journal of Superconductivity and Novel Magnetism. 2015;**28**(5):1551-1558. DOI: 10.1007/s10948-014-2872-x

[22] Liu Y, Drew MG, Liu Y. Preparation and magnetic properties of barium ferrites substituted with manganese, cobalt, and tin. Journal of Magnetism and Magnetic Materials. 2007;**323**:945-953. DOI: 10.1016/j.jmmm.2010.11.075

[23] Nazlan R, Hashim M, Ibrahim IR, Mohd Idris F, Wan Ab Rahman WN, Abdullah NH, et al. Influence of indium substitution and microstructure changes on the magnetic properties evolution of $Y_3Fe_{5-x}In_xO_{12}$ (x = 0.0 − 0.4). Journal of Materials Science: Materials in Electronics. 2015;**26**(6):3596-3609. DOI: 10.1007/s10854-015-2874-x

[24] Fatemeh B, Masoud R, Mehdi MP. Synthesis of $SrFe_{12}O_{19}/SiO_2/TiO_2$ composites with core/shell/shell nano-structure and evaluation of their photo-catalytic efficiency for degradation of methylene blue. Journal of Materials Science: Materials in Electronics. 2018;**29**(3):1877-1887

[25] Mangai KA, Sureshkumar P, Priya M, Rathnakumari M. Structural and magnetic properties of strontium hexa-ferrites for permenant magnets. International Journal of Scientific & Engineering Research. 2014;**5**(3):65-69

[26] Masoudpanah SM, Seyyed Ebrahimi SA. Effect of pH value on the structural and magnetic properties of nanocrystalline strontium hexaferrite thin films. Journal of Magnetism and Magnetic Materials. 2011;**323**(21):2643-2647. DOI: 10.1016/j.jmmm.2011.05.055

[27] Dang TMH, Trinh VD, Bui DH, Phan MH, Huynh DC. Sol-gel hydrothermal synthesis of strontium hexaferrite nanoparticles and the relation between their crystal structure and high coercivity properties. Advances in Natural Sciences: Nanoscience and Nanotechnology. 2012;**3**(2):25015

[28] Wang Y, Li Q, Zhang C, Li B. Effect of Fe/Sr mole ratios on the formation and magnetic properties of $SrFe_{12}O_{19}$ microtubules prepared by sol-gel method. Journal of Magnetism and Magnetic Materials. 2009;**321**(19):3368-3372. DOI: 10.1016/j.jmmm.2009.05.066

[29] Reza G, Ghasemi A, Saidi A. Enhanced magnetic properties of substituted Sr-hexaferrite nanoparticles synthesized by co-precipitation method. Ceramics International. 2014;**40**(3):4945-4952. DOI: 10.1016/j.ceramint.2013.10.096

[30] Malhotra S, Chitkara M, Sandhu IS. Microwave absorption study of nano synthesized strontium ferrite particles in X band. International Journal of Signal Processing, Image Processing and Pattern Recognition. 2015;**8**(10):115-120

[31] Maswadeh Y, Mahmood SH, Awadallah A, Aloqaily AN. Synthesis and structural characterization of nonstoichiometric barium hexaferrite materials with Fe:Ba ratio of 11.5–16.16. IOP Conference Series: Materials Science and Engineering. 2015;**92**:012019. DOI: 10.1088/1757-899X/92/1/012019

[32] Pereira FMM, Junior CAR, Santos MRP, Sohn RSTM, Freire FNA, ki JM, et al. Structural and dielectric spectroscopy studies of the M-type barium strontium hexaferrite alloys

($Ba_xSr_{1-x}Fe_{12}O_{19}$). Journal of Materials Science: Materials in Electronics. 2008;**19**(7):627-638. DOI: 10.1007/s10854-007-9411-5

[33] Song F, Shen X, Xiang J, Song H. Formation and magnetic properties of M-Sr ferrite hollow fibers via organic gel-precursor transformation process. Materials Chemistry and Physics. 2010;**120**(1):213-216. DOI: 10.1016/j.matchemphys.2009.10.048

[34] Sivakumar M, Gedanken A, Zhong W, Du YW, Bhattacharya D. Nanophase formation of strontium hexaferrite fine powder by the sonochemical method using $Fe(CO)_5$. Journal of Magnetism and Magnetic Materials. 2004;**268**:95-104. DOI: 10.1016/S0304-8853(03)00479-7

[35] Nazlan R, Hashim M, Abdullah NH, Ibrahim IR, Ismail I. Influence of milling time on the crystallization, morphology and magnetic properties of polycrystalline yttrium iron garnet. Advanced Materials Research. 2012;**501**:324-328. DOI: 10.4028/www.scientific.net/AMR.501.324

[36] Yang FJ, Min JJ, Kang ZW, Tu SY, Chen HB, Liu DG, et al. The influence of pH value and composition on the microstructure, magnetic properties of Co-Fe-Al Heusler nanoparticles. Chemical Physics Letters. 2017;**670**(3):1-4. DOI: 10.1016/j.cplett.2016.12.062

[37] Tian L, Xu J, Xiao S. The influence of pH and bath composition on the properties of Ni-Co coatings synthesized by electrodeposition. Vacuum. 2011;**86**(1):27-33. DOI: 10.1016/j.vacuum.2011.03.027

[38] Hesani M, Yazdani a, Abedi Ravan B, Ghazanfari M. The effect of particle size on the characteristics of FeCo nanoparticles. Solid State Communications. 2010;**150**(13–14):594-597. DOI: 10.1016/j.ssc.2009.12.043